Receptive Field Changes After Strokelike Cortical Ablation: A Role for Activation Dynamics

SAMUEL J. SOBER,[1,2] JEANNE M. STARK,[2] DWAYNE S. YAMASAKI,[2] AND WILLIAM W. LYTTON[1]

[1]*Department of Neurology and* [2]*Department of Anatomy, University of Wisconsin, William S. Middleton Veterans Hospital, Madison, Wisconsin 53706-1532*

Sober, Samuel J., Jeanne M. Stark, Dwayne S. Yamasaki, and William W. Lytton. Receptive field changes after strokelike cortical ablation: a role for activation dynamics. *J. Neurophysiol.* 78: 3438–3443, 1997. The reorganization of neural activity that takes place after stroke is of paramount importance in producing functional recovery. Experimental stroke models have suggested that this reorganization may have two phases, but physiology alone cannot fully resolve what causes each phase. Computer modeling suggests that these phases might involve an initial change in dynamics occurring immediately, followed by synaptic plasticity. We combined physiological recording from macaque middle temporal cortex (area MT) with a neural network computer model to examine this first phase of altered cortical function after a small, experimentally induced cortical lesion. Major receptive field (RF) changes seen in the first few days postlesion included both expansion and contraction of receptive fields. Although only expansion could be reproduced in an initial model, addition of inhibitory interneuron loss in a ring around the primary ablation, suggested by immunohistochemical examination, permitted contraction to be replicated as well. We therefore predict that this immunochemical observation reflects an immediate extension of the lesion rather than a late response. Additionally our model successfully predicted a correlation between increased firing rate and RF size. Our model suggests that activation dynamics alone, without anatomic remodeling, can cause the large receptive field changes that allow the rapid behavioral recovery seen after middle temporal lesions.

INTRODUCTION

Stroke recovery involves a process of neural reorganization thought to follow the same principles involved in development of the immature nervous system (Armentrout et al. 1994; Goodall et al. 1997). In development, neural connectivity is believed to be progressively refined based on a Hebbian mechanism, with synaptic strength changes determined by underlying activity in pre- and postsynaptic neurons (Miller et al. 1989; Miller 1994). Similarly, cortical maps damaged by ischemia are known to reorganize over a period of months, presumably by activity-dependent changes in synaptic efficacy (Jenkins and Merzenich 1987). Although most studies focus on physiological and anatomic remodeling occurring over long periods, a full understanding requires attention to the acute changes in neural activity that shape synaptic modification. With the resultant synaptic changes determined by earlier patterns of activity, these immediate changes in neural activation dynamics will have long-term consequences of utmost importance for restoration of function.

Animal models of stroke have, in fact, suggested that postablation recovery has two phases (Nudo et al. 1996;

Nudo and Milliken 1996; Wurtz et al. 1990). Behaviorally, some degree of recovery is seen immediately followed by a plateau phase or, in some cases, a transient worsening in function (Nudo et al. 1996). Thereafter, further recovery to a final plateau is seen. This suggests that reorganization might involve an initial phase of simple dynamical alterations in neural activation (activation dynamics), followed by a plasticity phase where synaptic strengths are recast. Independently, computer modeling studies have also suggested two phases. These two modeling phases are a logical consequence of the observation that, if Hebbian mechanisms are to cause alterations in synaptic weights, an initial change in pattern of activity must precede these alterations. In the case of an ablation model, this immediate change in neural activation dynamics will be a direct consequence of the ablation, as the underlying steady-state dynamics of the fully developed system is disrupted by the loss of some elements.

In this study, physiological measurements of neurons surviving small lesions in macaque middle temporal visual area (area MT) show dramatic alterations in receptive fields and firing rates. We utilize a computer model to determine whether or not these changes could be explained on the basis of dynamics alone, without rewiring.

METHODS

Receptive field (RF) data were obtained from three hemispheres of two awake, behaving rhesus monkeys both before and after electrolytic or chemical lesioning. All animal care and usage was approved by the University of Wisconsin's Research Animals Resource Committee and conformed to the requirements of the National Institutes of Health, as well as the U.S. Department of Agriculture Animal Welfare Act. Over 200 postlesion neurons were mapped, of which 173 were fully quantified. 18 neurons were recorded during the acute postlesion period that was emphasized in the current study. For the purpose of data analysis, all RFs larger than prelesion mean were considered expanded and all those smaller than prelesion mean contracted. Motion scotomata determined both physiologically and behaviorally were well correlated.

In each hemisphere, middle temporal visual area (MT) and medial superior temporal area (MST) boundaries were determined. Guide tubes (GTs) were lowered at several sites ~3 mm above the dorsal border of MST (Crist et al. 1988), permitting examination of the same location both before and after a lesion. Repeated sampling of cells from each GT prelesion showed RFs of similar size and eccentricity, providing assurance that the same subpopulation was being assayed pre- and postlesion. Single neuron activity was isolated (BAK Electronics window discriminator, Tektronix oscilloscopes, Grass Instruments audio amplifier). RFs were mapped with a light spot or slit during a standard fixation task monitored by eye
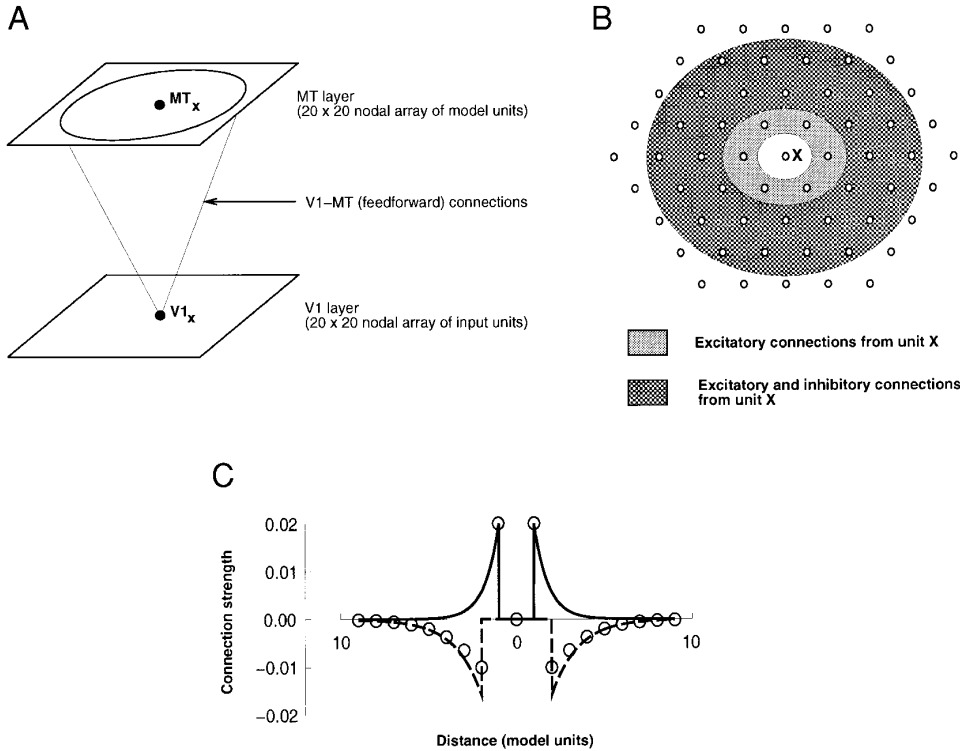
FIG. 1. Network schematic. *A*: model architecture. Both primary visual area (V1) and MT layers are two-dimensional arrays of nodes. States of V1 units are inputs that are held constant for duration of a trial. Feedforward connections are divergent and are strongest between units occupying homologous positions ($V1_X$, and MT_X). Strength of feedforward connections declines with lateral distance according to a Gaussian function (*Eq. 3*). *B*: lateral connectivity in middle temporal cortex (MT) layer: each unit has both excitatory and inhibitory connections to other units in layer. Units make exclusively excitatory connections to their nearest neighbors (gray region). Connections to more distant units are both excitatory and inhibitory (stippled region), but have an overall inhibitory influence. *C*: lateral connectivity in MT layer: excitatory (——, *Eq. 4*), inhibitory (– – –, *Eq. 5*), and summed (○) connection strengths.

coils (Wurtz 1969). Chemical (DL-α-amino-3-hydroxy-5-methyl-isoxazole-4-propionate [AMPA], Sigma Chemical) and electrolytic lesions were made by using lesion protocols previously described (Yamasaki and Wurtz 1991). Repeated recording from GTs postlesion allowed us to estimate the spatial and temporal course of cell death. Neuronal mortality resulting from electrolytic lesion appeared to be complete within 24 h. When AMPA lesions were used, cell death appeared to continue over a full week. No GTs with ongoing cell death are included in the presented data. Viable GTs were found at distances ranging from 1.4 to 5.0 mm from the injection/electrolytic site. By using the small ($n = 7$) number of sampled guide tubes, we made an order of magnitude estimation of 10 mm for lesion size. Anatomic verification of the sizes was not yet obtained. With the range of distances sampled, we believe that we obtained recordings from cells both within and beyond the inhibitory halo.

A simple single-layer neural network, based closely on previous models of sensory cortex (Cho and Reggia 1994; Reggia et al. 1992; von der Malsburg 1973) was adapted to represent MT receiving retinotopic inputs from primary visual area V1 (Fig. 1*A*). Both the output layer (representing area MT) and its inputs (representing V1) consisted of 400 units (20 × 20), hexagonally tessellated nodal arrays (Reggia et al. 1992; Cho and Reggia 1994; von der Malsburg 1973). Individual MT units represented populations of neurons and postlesion changes in model unit responses represented changes averaged across a neuronal population. Activity (a_k) of MT *unit k* was defined by

$$da_k/dt = -a_k \cdot \tau + \phi(a_k) \left(\sum_{i=1}^{400} V_{ki} b_i + \sum_{i=1}^{400} M_{ki} a_i \right) \quad (1)$$

$$\phi(a_k) = -4(a_k^2/A - a_k) \quad (2)$$

with $\tau = 0.2$ and $A = 5$, where the *V* weight matrix was the projection from V1 to MT, b_i were inputs from V1, and the *M* weight matrix expressed lateral connectivity within MT. Function $\phi(a_k)$ was used to eliminate drive when unit activity approached 0 or *A*, thereby keeping a_k within these bounds. This function

yielded input/output curves for model units similar to those commonly used (Reggia et al. 1992; Sutton et al. 1994), with an asymptote at A, but added an initial region of low gain, which simulated the aggregate relative thresholds of a population of neurons. During simulation, a small proportion (5–10%) of heavily inhibited units was bounded by $\phi(a_k)$ at $a_k = 0$, whereas no units reached the upper bound. Connections from V1 to MT units were made to diverge widely, corresponding to anatomic findings concerning the arborization pattern of axons projecting from V1 to MT (Rockland 1989). This projection was topographic with wraparound to prevent edge effects. The elements of matrix *V* were excitatory (positive) and calculated from radial coordinates *r* of the hexagonally tessellated units. Divergence from a given V1 location to the MT units had Gaussian spatial falloff

$$V(r) = k \cdot e^{-1/2(r/s)^2} \quad (3)$$

where *k* was a normalizing constant and *s* was the divergence parameter (Reggia et al. 1992). In all data except that shown in Fig. 2*C*, $s = 3.0$ and $k = 1.0$.

Similarly, *M* was calculated from excitatory $E(r)$ and inhibitory $I(r)$ functions with wraparound (Fig. 1, *B* and *C*). Lateral excitatory connections were highly divergent and declined in strength exponentially

$$E(r) = c \cdot e^{-r/\lambda} \quad (4)$$

with $c = 0.02$, $\lambda = 0.8$, $r \geq 1$ (no self-connection).

Lateral inhibition in the model represented small inhibitory interneurons conceptualized as receiving excitation from distant excitatory units and providing local inhibition (Celio 1986). Therefore loss of inhibitory interneurons was modeled as a reduction in negative connection strength onto local MT units. Lateral inhibition was offset to form the Mexican hat

$$I(r) = c \cdot e^{-(r-1)/\lambda} \quad (5)$$

with $c = 0.0157$, $\lambda = 1.5$, and $r \geq 2$.

A receptive field was calculated by serially activating each of the 400 inputs and recording whether or not the given MT unit responded above threshold ($\theta = 0.5$). For simple ablations, units were eliminated from the model by locking their states at zero. For disinhibitory halo ablations, this lesion was surrounded by a zone in which inhibitory connections were reduced by a constant percentage. Bicuculline application was simulated by similar reductions in inhibitory connections in a limited area.
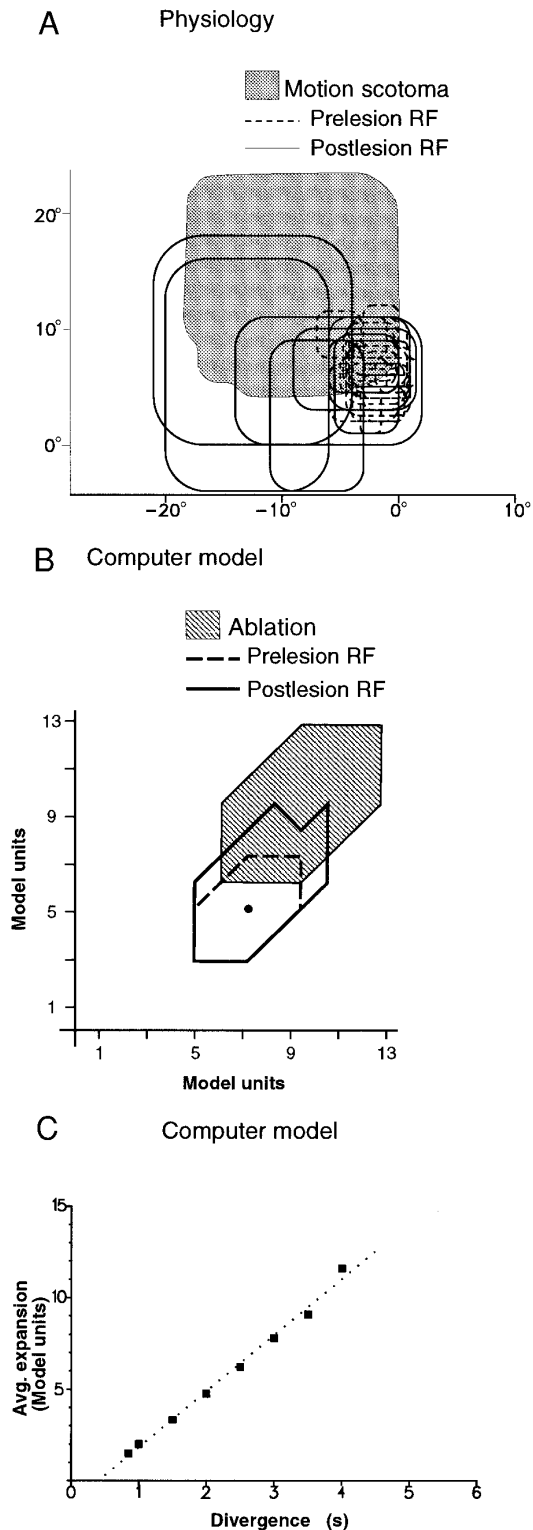
Equations were solved by using Runge-Kutta integration in MATLAB on a Silicon Graphics Indy workstation. Evaluation of all 400 RFs for a particular simulation took about 4 h of CPU time.

RESULTS

Physiologically, receptive field expansions in the macaque were seen soon after lesioning (3 h–3 days) and had an average expansion of 2.2 times the prelesion RF size mean (range 1.1–7.0; $n = 13$). In 75% of the cases where acute expansion was seen, the expansion was asymmetric (Fig. 2A), with the expansion generally toward the scotoma (the area previously represented by the lost neurons). In addition to expansion, RF shift was seen. RF contraction was also seen shortly after lesions (Fig. 3A); average contraction was 0.49 times the prelesion RF mean (range 0.22–0.80; $n = 5$).

Modeled lesions, representing loss of both pyramidal cells and GABAergic interneurons, also produced expanding RFs with expansion toward the lost units (Fig. 2B). The model showed that the magnitude of expansion correlated with the degree of V1-MT divergence (Fig. 2C). High divergence produced large postlesion RF expansion, because ablation unmasked weak connections from V1, which were previously hidden because of lateral inhibition within MT. The modeled expansion was most pronounced in those MT units close to the lesion, which lost more inhibitory connections.

Although this model replicated the more commonly seen expanding RFs, it did not reproduce physiologically observed RF contraction (Fig. 3A). We looked to the microanatomy of one of the cortical lesions made in the physiological experiments to explain this discrepancy. Brain sections from one macaque killed 62 days postlesion revealed a graded loss of calbindin and parvalbumin labeled cells in layers II, III, and IV within 1 to 2 mm of the lesion (K. Huxlin and W. Merigan, personal communication). Because these labels are believed to be specific to GABAergic neurons (Blumcke et al. 1994; Celio 1986; Hendry et al. 1989), this suggested the existence of a halo of inhibitory neuron loss surrounding the ablated area.

Assuming that this cell loss was a direct effect of the ablation, we modified the model by surrounding the central ablation by a disinhibitory halo (Fig. 3, B and C). This new model produced a wider variety of RF effects, including both RF expansion and contraction. In addition, in the new model, RF expansions observed within the disinhibited zone were much larger than those seen with the original model. This further expansion was the result of the greater disinhibi-

FIG. 2. Expansion of receptive fields after lesion. A: multiple MT receptive fields (RFs) recorded from a single guide tube. Each RF depicted is from a single cell and is represented in degrees of visual space. RF size was measured vertically and horizontally; precise RF shape was not systematically determined. RFs depicted here were recorded from 3 h to 3 days after lesion. RF changes were generally consistent across this period of time. B: computer model shows expansion of a single RF. Model V1 (inputs) and model MT (unit layer) are of same size and are mapped together. Ablation shown is zone where MT units are removed. C: model RF expansion correlates with V1-MT divergence used. Abscissa: range of tested values of spatial decay constant of Gaussian function (Eq. 3) used to generate feedforward connection strengths. Abscissa is V1-MT divergence parameter s in Eq. 3. Ordinate is average increase in RF size after a 6 unit diameter lesion. $V(r)$ was normalized to maintain prelesion RF size.
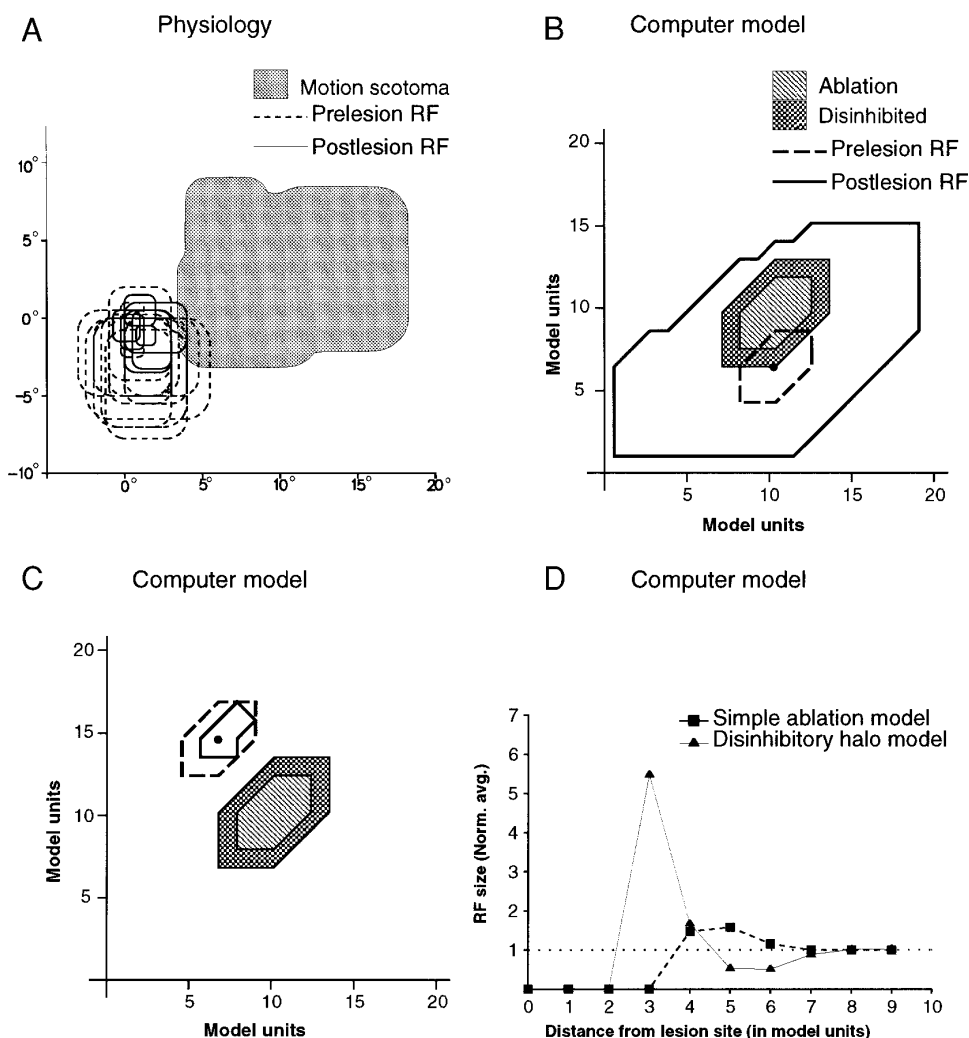
FIG. 3. Contraction of receptive fields after lesion. *A*: MT RF contraction from a single guide tube (GT). All RFs shown were recorded in 1st 3 days postlesion. Conventions same as in Fig. 1*A*. *B*: ablation with disinhibition produced large RF expansion at edge of ablation. Disinhibitory halo generated by weakening incoming inhibitory connections by 40%. *C*: RF contraction occurred at a distance from ablation area. *D*: comparison with previous computer model showed that disinhibitory halo model produced larger RF expansions and also produced RF contractions not seen in simple ablation model. These effects were robust across a range of lesion diameters, values of *s* in *Eq. 3* and to randomization of individual disinhibition strengths.

tion in the new model and was fairly symmetrical (Fig. 3*B*). RF expansion in model units neighboring the disinhibited zone showed the previously demonstrated elongation toward the lesion (not shown). RF contraction was observed in model units at greater distance from the ablation and was nondirectional (Fig. 3*C*).

In the model, these three effects (RF expansion, RF contraction, and asymmetrical RF expansion) can all be explained as primary or secondary dynamical effects of disinhibition (Fig. 3*D*). Model units that are in the disinhibitory halo immediately expand omnidirectionally because they no longer receive significant lateral inhibition. They therefore can respond even to very weak V1 afferents. These highly excitable units in turn cause RF shrinkage in distant cells via their intact lateral inhibitory connections. In between these two extremes are model units that were elongated toward the lesion because of reduced inhibition and secondary excitation on the near-ablation side, with increased inhibition on the distant side.

Exploration of the model revealed an interesting correlation between maximum response and receptive field size. Model units with RF expansions showed an increase in maximum response compared with their prelesion status, whereas

units with RF shrinkage showed a decrease (Fig. 4*A*). We predicted that similar findings might be found physiologically by comparing changes in maximum evoked firing rate to change in RF size. The physiological data were consistent with this tendency; the sign and magnitude of RF change correlated with the sign and magnitude of the maximum evoked firing rates of the cells recorded from that guide tube (Fig. 4*B*). The physiological confirmation of the model's prediction is further evidence that activation dynamics rather than synaptic changes could be responsible for acute changes in neuronal response to the stimulus. This result was robust in the face of randomized reduction of individual inhibitory strengths.

In addition, we isolated the effect of disinhibition in the model by simulating focal application of a GABAergic antagonist such as bicuculline in our model. As expected, the model produced large RF expansions in the disinhibited area, with RF contraction beginning at the edge of the disinhibitory effect and diminishing with distance (not shown). Bicuculline was reported to cause dramatic RF expansion in the area of application (Dykes et al. 1984). Our model predicts that RF contraction would be found just outside this area.
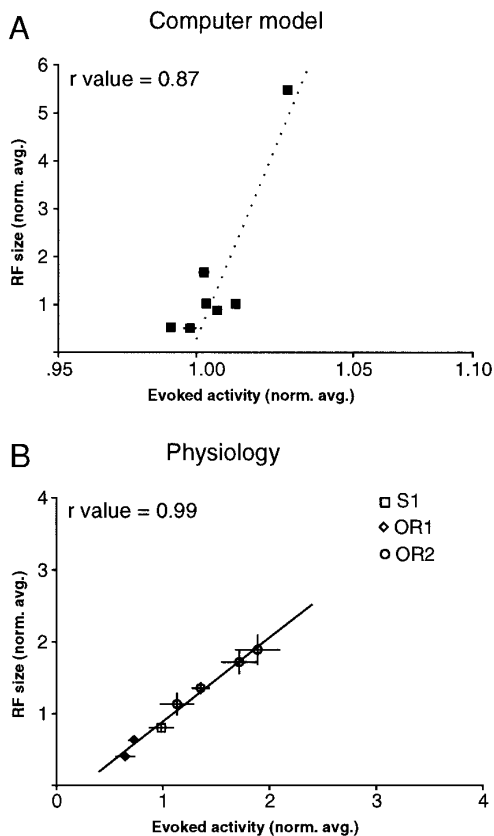
FIG. 4. Positive correlation between RF size and maximum response. *A*: postablation RF size correlated with maximum evoked activity. Each point represents normalized, averaged maximum response of all units a given distance ($r = 3–9$) from center of lesion surrounded by a halo of 60% disinhibition. Standard error bars are hidden by symbols. This effect was robust across a range of lesion diameters, values of *s* in *Eq. 3* and to randomization of individual disinhibition strengths. *B*: physiological data for all GTs that remained viable for duration of experiment. Each value shown is from a single GT, with RF data pooled across all days studied. Individual cell figures from each GT were normalized to prelesion mean and averaged. Normalization for RF size used all prelesion cells; for evoked activity, only same hemisphere cells were used. Different symbols correspond to different hemispheres from 2 monkeys (S and OR). Trend is statistically significant.

DISCUSSION

Our physiological results confirm predictions of previous computational models that showed enlarged postlesion RFs (Sutton et al. 1994). Our disinhibitory halo model, based on immunohistochemistry, additionally provides an explanation for RF contraction and makes an accurate prediction regarding firing rates. We predict from the model that interneuron loss must occur during the first three days postlesion. Anatomic analysis performed at short time intervals after a lesion will permit us to test this prediction. Evidence for excessive interneuron death in an area of ischemic lesion was reported in hippocampal area CA1 in an animal model of stroke (De Jong et al. 1993).

Certain physiological observations did not concord with the model: *1*) physiological RF elongation was not consistently toward the lesion; *2*) the location of contracting and expanding RFs relative to the lesion was not consistent; and *3*) RF shift was seen physiologically, but was not explained by the current model. Because these are discrepancies that can be explained by statistical effects, we believe that much of this variability could be reproduced in a model of larger size by randomizing the connection weights to reflect the nonuniformity of the biological network. Additionally, the topography of RF changes would be expected to depend strongly on asymmetries of excitotoxin injection or electrolytic orientation that could also be incorporated into the model. Finally, whereas the simulated lesions were instantaneous, physiological cell death, particularly that resulting from ischemia, is an ongoing process that would contribute its own dynamics to the overall response (Goodall et al. 1997).

Although the minimum time required for synaptic changes to occur is not clear at present, the ability of purely dynamical changes to account for most of the observed phenomena suggests that activation dynamics may be primarily responsible for cellular responses seen in the first few days after ablation. Although these activity changes might be regarded as ''dynamic plasticity,'' they should be clearly distinguished from synaptic or other structural changes that are more properly plastic adaptations.

Dynamic expansion of cortical receptive fields may be an adaptive response to stroke that helps preserve function by filling in for lost cells. Additionally, the combined effects of increased firing and increased receptive field size might be expected to predispose to subsequent synaptic strength changes associated with functional recovery. Further understanding of the interplay of early dynamics and subsequent synaptic changes may suggest new strategies to promote recovery from stroke.

REFERENCES

ARMENTROUT, S. L., REGGIA, J. A., AND WEINRICH, M. A neural model of cortical map reorganization following a focal lesion. *Artif. Intell. Med.* 6: 383–400, 1994.

BLUMCKE, I., WERUAGA, E., KASAS, S., HENDRICKSON, A. E. AND CELIO, M. R. Discrete reduction patterns of parvalbumin and calbindin d-28k immunoreactivity in the dorsal lateral geniculate nucleus and the striate cortex of adult macaque monkeys after monocular enucleation. *Vis. Neurosci.* 11: 1–11, 1994.

CELIO, M. R. Parvalbumin in most gamma-aminobutyric acid-containing neurons of the rat cerebral cortex. *Science* 231: 995–997, 1986.

CHO, S. AND REGGIA, J. A. Map formation in proprioceptive cortex. *Int. J. Neural Syst.* 5: 87–101, 1994.

CRIST, C. F. YAMASAKI, D. S., KOMATSU, H., AND WURTZ, R. H. A grid system and a microsyringe for single cell recording. *J. Neurosci. Methods* 26: 117–122, 1988.

DE JONG, G. I., VAN DER ZEE, E. A., BOHUS, B., AND LUITEN, P.G.M. Reversed alterations of hippocampal parvalbumin and protein kinase c-gamma immunoreactivity after stroke in spontaneously hypertensive stroke-prone rats. *Stroke* 24: 2082–2085, 1993.

DYKES, R. W., LANDRY, P., METHERATE, R., AND HICKS, T. P. Functional

role of GABA in cat primary somatosensory cortex: shaping receptive fields of cortical neurons. *J. Neurophysiol.* 52: 1066–1093, 1984.

GOODALL, S., REGGIA, J. A., CHEN, Y. N., RUPPIN, E., AND WHITNEY, C. A computational model of acute focal cortical lesions. *Stroke* 28: 101–109, 1997.

HENDRY, S. H., JONES, E. G., EMSON, P. C., LAWSON, D. E., HEIZMANN, C. W., AND STREIT, P. Two classes of cortical GABA neurons defined by differential calcium binding protein immunoreactivities. *Exp. Brain Res.* 76: 467–472, 1989.

JENKINS, W. M. AND MERZENICH, M. M. Reorganization of neocortical representations after brain injury: a neurophysiological model of the bases of recovery from stroke. *Prog. Brain Res.* 71: 249–266, 1987.

MILLER, K. D. A model for the development of simple cell receptive fields and the ordered arrangement of orientation columns through activity-dependent competition between on- and off-center inputs. *J. Neurosci.* 14: 409–441, 1994.

MILLER, K. D., KELLER, J. B., AND STRYKER, M. P. Ocular dominance column development: analysis and simulation. *Science* 245: 605–615, 1989.

NUDO, R. J. AND MILLIKEN, G. W. Reorganization of movement representations in primary motor cortex following focal ischemic infarcts in adult squirrel monkeys. *J. Neurophysiol.* 75: 2144–2149, 1996.

NUDO, R. J., WISE, B. M., FUENTES, F., AND MILLIKEN, G. W. Neural sub-strates for the effects of rehabilitative training on motor recovery after ischemic infarct. *Science* 272: 1791–1794, 1996.

REGGIA, J., D'AUTRECHY, C., SUTTON, G., AND WEINRICH, M. A competitive distribution theory of neocortical dynamics. *Neural Comput.* 4: 287–317, 1992.

ROCKLAND, K. S. Bistratified distribution of terminal arbors of individual axons projecting from area V1 to middle temporal area (MT) in the macaque monkey. *Vis. Neurosci.* 3: 155–170, 1989.

SUTTON, G., REGGIA, J., ARMENTROUT, S., AND D'AUTRECHY, C. Cortical map reorganization as a competitive process. *Neural Comput.* 6: 1–13, 1994.

VON DER MALSBURG, C. Self-organization of orientation sensitive cells in the striate cortex. *Kybernetik* 14: 85–100, 1973.

WURTZ, R. H. Visual receptive fields of striate cortex neurons in awake monkeys. *J. Neurophysiol.* 32: 727–742, 1969.

WURTZ, R. H., YAMASAKI, D. S., DUFFY, C. J., AND ROY, J. P. Functional specialization for visual motion processing in primate cerebral cortex. *Cold Spring Harb. Symp. Quant. Biol.* 5: 717–727, 1990.

YAMASAKI, D. S. AND WURTZ, R. H. Recovery of function after lesions in the superior temporal sulcus in the monkey. *J. Neruophysiol.* 66: 651–673, 1991.